

THE MECHANICAL NATURE OF STRESS-CORROSION
CRACKING IN Al-Zn-Mg ALLOYS: I. EVALUATION OF
THE DUCTILE RUPTURE CONTRIBUTION

W. E. Wood and W. W. Gerberich

RECEIVED
LAWRENCE
RADIATION LABORATORY

JAN 2 1974

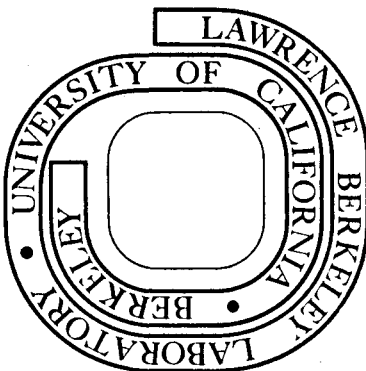
November 1973

LIBRARY AND
DOCUMENTS SECTION

Prepared for the U. S. Atomic Energy Commission
under Contract W-7405-ENG-48

For Reference

Not to be taken from this room



DISCLAIMER

This document was prepared as an account of work sponsored by the United States Government. While this document is believed to contain correct information, neither the United States Government nor any agency thereof, nor the Regents of the University of California, nor any of their employees, makes any warranty, express or implied, or assumes any legal responsibility for the accuracy, completeness, or usefulness of any information, apparatus, product, or process disclosed, or represents that its use would not infringe privately owned rights. Reference herein to any specific commercial product, process, or service by its trade name, trademark, manufacturer, or otherwise, does not necessarily constitute or imply its endorsement, recommendation, or favoring by the United States Government or any agency thereof, or the Regents of the University of California. The views and opinions of authors expressed herein do not necessarily state or reflect those of the United States Government or any agency thereof or the Regents of the University of California.

THE MECHANICAL NATURE OF STRESS-CORROSION CRACKING IN
Al-Zn-Mg ALLOYS: I. EVALUATION OF THE
DUCTILE RUPTURE CONTRIBUTION*

W. E. Wood** and W. W. Gerberich**

ABSTRACT

A detailed study of rapid stress-corrosion-cracking (SCC) in a 7075 aluminum alloy has allowed separation of the mechanical and chemical contributions. This was accomplished by combining scanning electron microscopy, stress-wave emission and crack growth rate observations as a function of test temperature. These established an activation energy of 11.2 kcal/mol, a stress-intensity squared dependence of crack growth, and a range of 20-80% dimpled rupture on the fracture surfaces. Thus a two-step crack growth mechanism is proposed combining a thermally activated electrochemical process and a discontinuous mechanical jumping process.

* This research was performed at the Inorganic Materials Research Division, Lawrence Berkeley Laboratory, and Department of Materials Science and Engineering, College of Engineering, University of California, Berkeley, California 94720.

** Presently assistant professor of Materials Science at the Oregon Graduate Center in Beaverton, Oregon 97005, and associate professor of Materials Science at the University of Minnesota, Minneapolis, Minn. 55455, respectively.

INTRODUCTION

The case for the type of stress-corrosion-cracking (SCC) mechanism in aluminum alloys has oscillated between those who advocate a purely electrochemical dissolution process⁽¹⁻⁵⁾ and those who advocate a combined electrochemical-mechanical process.⁽⁶⁻⁹⁾ From an electrochemical viewpoint, most explanations involve localized dissolution at anodic sites such as precipitate particles, e.g. $MgZn_2$, or emerging slip bands within the precipitate free zone (PFZ). A combined mechanism adds in some discontinuous brittle or ductile rupture process so that the overall mechanism is an alternating two-step process. A subset problem area has been whether or not the PFZ width of high-strength aluminum alloys plays a major role in the process.⁽¹⁰⁻¹²⁾ Although considerable work has been done on electrochemical and PFZ aspects, there have been relatively few quantitative attempts to determine the extent of micro-mechanical contributions to SCC except for the theoretical model proposed by Krafft and Mulherin.⁽⁸⁾

The following study of 7075 aluminum was designed to attempt a detailed definition of the mechanical aspect of the SCC mechanism. First, a recrystallization treatment to aid in providing a reasonable grain-boundary path and a low pH solution were utilized to promote rapid SCC. Second, the initiation stage was eliminated by starting with a pre-fatigue cracked, edge-notched specimen. Third, crack propagation rates were determined as a function of stress intensity factor to obtain a better mechanical description of the growth process. Fourth, tests were run at a relatively constant stress intensity level as a function of test temperature to define the activation energy of the thermally

activated mechanism. Finally, a stress-wave emission (SWE) technique to monitor any discontinuous crack jumps and scanning electron microscopy were utilized to separate out mechanical and chemical contributions to the growth process.

EXPERIMENTAL PROCEDURE

Commercially obtained 7075 aluminum alloy was first cold rolled from .080" to .060" in thickness and then solution heat treated at 500°C for 3 days and quenched in water at 82°C, resulting in a cooling rate of about 65°C per second.⁽¹³⁾ The material was then aged for 5 days at 88°C to a -T6 temper which has been reported⁽¹⁴⁾ as leading to an increased susceptibility to stress corrosion cracking.

To verify the properties of the as-received alloy as well as the cold worked and heat treated alloy, standard tensile tests were done. For the SCC tests, single edge notched specimens were machined with their tensile axis perpendicular to the grain orientation of the sheet. The specimen geometry selected is that given by Brown and Srawley,⁽¹⁵⁾ for which the stress intensity factor may be given in terms of load, P, crack length, a, thickness, B, and width, W, by

$$K = Y \frac{Pa^{1/2}}{BW} \quad (1)$$

with Y being the finite width correction factor,

$$Y = 1.99 - 0.41 (a/W) + 18.70 (a/W)^2 - 38.48 (a/W)^3 + 53.85 (a/W)^4 \quad (1a)$$

The SEN specimens were pre-fatigue cracked in a tension-tension fatigue machine at a Δk of 13 ksi-in^{1/2} to introduce a crack in approximately 15,000 cycles.

The SCC tests were done in a 3.5% NaCl solution with AlCl₃ added to lower the pH of the solution to less than two. In order to determine the crack growth rate as a function of temperature, the NaCl + AlCl₃ solution was heated to a controlled temperature, and then allowed to flow slowly through a plastic tubing and past the notched area of the SEN specimen. A thermometer was inserted into the tubing close to the specimen in order to actually measure the temperature of the solution as it passed the specimen.

Elastic stress waves are caused by the discontinuous growth of a crack before catastrophic failure. By using a suitable piezoelectric transducer attached to the specimen grips, these emissions can be detected, if they are within the sensitivity range of the instrument. The stress wave emission technique developed by Hartbower et al.⁽¹⁶⁻¹⁸⁾ has been used to study the behavior of slow crack growth propagation in SEN specimens, and provides an extremely sensitive method for monitoring stress-wave emission produced by discontinuous crack growth. The complete instrumentation and test apparatus is shown schematically in Fig. 1. As the signal is the result of a very small amount of energy being released by a discontinuous crack movement, it is necessary to amplify it and to filter out extraneous noise. After the test was over, the taped signal was played back at 7-1/2 ips (at one-half speed and thus one-half of the highest recorded frequency), so as to be well within the frequency response of the galvanometer (5kHz) utilized in the recording

oscillograph. The resulting gain of the system comprising the charge amplifier, voltage amplifier, and the recorder amplifier of 1 to 3, was approximately 112,500.

Standard metallographic techniques were used to examine the microstructure of the as-received material in comparison to the cold worked and heat treated material. The scanning microscope (SEM) employing secondary electron emission at 25 kV was used to study the fracture surface of the specimens over a range of magnification from 200X to 20,000X.

EXPERIMENTAL RESULTS AND OBSERVATIONS

Typical microstructures, as shown in Fig. 2, indicate the as-received material contained about 250 grains across the thickness, or a grain width of about 12.5 microns. After cold rolling and heat treating, there were about 70 grains across the thickness or a grain width of about 22 microns. The grain length did not change between the two conditions and averaged about 100 microns. Five tensile tests each of both conditions gave the average results in Table 1.

SCC tests were done at different load levels for short intervals of crack growth so that both K and $\frac{da}{dt}$ could be determined. Due to the geometry of the SEN specimen, the stress intensity level increases and the crack grows. Thus, for these tests, the initial value, K_0 , and the final value, K_f , were calculated and an average value assumed. In order that there be only a small change in the stress intensity during the test, the tests were run long enough so that there would be a relatively small amount of crack growth. This also had the advantage of allowing little time for additional corrosion of the exposed fracture surfaces.

The specimens were then broken by loading at 0.13 in/min so that the amount of slow crack growth could be determined. Figure 3 shows a log-log plot of the stress intensity versus the slow crack growth rate. The slope of the curve, determined by a least square analysis on an IBM computer, was found to be equal to 2. No crack growth was observed (after 328 minutes) at a stress intensity of 9250 psi-in^{1/2}.

Tests were performed to determine the dependence of the slow crack growth rate on the temperature of the environment. The results are given in Table 2 and shown in Fig. 4 for three different stress intensity levels. Again, a least squares analysis was done to determine the best curves that could be drawn through the data points. From the equation

$$\frac{da}{dt} = Ae^{-Q/RT} \quad (2)$$

the activation energy, Q, can be computed from the slope of the curves. The average value of the apparent activation energy was found to be 11.2 kcal/mol.

Stress wave activity was observed in all the tests where slow crack growth occurred. Figure 5 shows some representative oscillogram recordings of the monitored waves and Table 3 indicates the dependence of the amplitude and frequency of the stress waves on the stress intensity. Due to the sensitivity of the system, the bubbles formed by the reaction of the environment with the material, produced a noise, which at elevated temperatures made it impossible to distinguish between real stress waves and the wave produced by the bubbles. Even at 48°C the noise of the

bubbles made it impossible to identify the stress waves. However, at 33°C and below, bubbles did not significantly raise the background noise, and allowed stress waves to be observed as a function of stress intensity. For example, Fig. 5 shows that the background noise level is negligible compared to the stress waves observed during SCC tests. The number of stress waves per second taken from data stored on the tapes, is only of the major waves. The real SWE activity might possibly be somewhat higher, involving more low energy waves. The average amplitude of the stress waves for each test was obtained from the amplitude of the six biggest waves in a given time interval.

Qualitatively then, the SWE observations show that as the stress intensity increases, the frequency and amplitude of the stress waves increases. Estimates of the incremental area swept out by the crack have been made by Gerberich and Hartbower.⁽¹⁶⁾ Quantitatively, a relationship between the incremental crack growth and stress wave activity has been suggested by Gerberich and Desai.⁽¹⁹⁾ Based on experimental work on an Al-Zn-Mg alloy and a theoretical compliance analysis, they derived a semi-empirical relationship of the form

$$g = \frac{2.5 CK_w^{1/2} \Delta A}{YB e} \quad (3)$$

where g is the amplitude of a stress wave, ΔA is the incremental area swept out by a crack as associated with one stress wave, e is the distance between loading pins, C is a constant of about 0.05, B is the specimen thickness, and Y is the $f\left(\frac{a}{W}\right)$ appropriate to the specimen configuration. By carefully calibrating the instruments shown schematically in Fig. 1,

the amplitude of the stress waves can be expressed in terms of g . For the settings used in these tests a stress wave amplitude of 1.9 inch is equal to .0008 g. Table 3 shows the calculated values of g and ΔA for different stress intensity levels based on Eq. (3).

Next, consider the metallographic observations. Figure 6 shows representative macroscopic fracture features for all the tests. Indicated on the figure is the pre-fatigue cracked region (A-B), the slow crack growth region (B-C), and the unstable crack growth region (C-D). Figures 7-10 show the microscopic details of the fracture surfaces. At low temperatures, the time of the tests was longer, and therefore the solution was in contact with the fracture surface for longer periods of time, thus destroying many of the fine details. This made it difficult to find any areas of dimpled rupture that might have been present initially. However, at high temperatures with shorter exposure times to the environment, fine detail can be observed. Figure 7 shows the two general types of morphology observed: (A) a relatively flat smooth surface and (B) a dimpled rupture type surface. A comparison of Figs. 8 and 9 shows that as the stress intensity level increases, the amount of dimpled rupture also increases. The dimpled regions represent discontinuous jumping or tearing of the material, as compared with the relatively flat surfaces which might be indicative of electrochemical dissolution. Besides the two general characteristics of the fracture process, there were also some artifacts on the fracture surface due to fracture of precipitated salts. For example, Fig. 10 (A-B) clearly shows one region of a test specimen containing what seemed to be deposits of the solution. This was verified by taking the solution, drying it on a

nickel plate, and examining it under the scanning electron microscope. As seen in Fig. 10 (C-D), the features of the residue are perfectly smooth with no texture present; the cracks in the residue are formed as the solution dries. Comparing Fig. 10(C) to Fig. 10(B) at the same magnification strongly indicates that this feature is not characteristic of the fracture surface and is merely a result of fractured salt crystals.

DISCUSSION

Those investigators⁽¹⁻⁵⁾ favoring a purely electrochemical process have considered how either matrix slip bands or a preferred slip in the PFZ might assist anodic dissolution. On the other hand, there are those⁽²⁰⁾ who have suggested that a grain-boundary crack is nucleated mechanically, and then propagates by an electrochemical mechanism or, alternatively,⁽²¹⁾ is nucleated by an electrochemical mechanism and then propagates mechanically. Various modifications of these with the influence of precipitate particles as the dissolution site have also been proposed.⁽¹⁴⁾ A recent review of most of these mechanisms has been presented,⁽²⁾ and thus a reiteration will not be attempted here. However, it is useful to reconsider those mechanisms with respect to the present findings.

First, one can state unequivocally from this study, that:

(1) The site for the SCC process is in or at the interface of the PFZ.

(2) A thermally-activated mechanism controls the rate of crack growth.

(3) The crack growth rate increases with increasing stress intensity.

(4) Fractographic and stress-wave emission studies show that the crack growth process is discontinuous, with mechanical rupture being a significant part of the growth mechanism.

All mechanisms are compatible with the first point. The second point suggests a thermally-controlled corrosion and/or diffusion process, which is also compatible with all mechanisms. The third point would be a little difficult to understand if only an electrochemical dissolution process were involved. One could argue that with higher stress intensity factors, there are more sites, e.g., greater frequency of slip bands, and hence more rapid anodic dissolution. However, in lieu of additional evidence, it is more satisfying to consider that the excess mechanical energy results in larger amounts of mechanical rupture. At least for the present investigation, the previous point is clarified by the fourth point which definitely confirms the discontinuous, mechanical feature of the SCC process.

Mechanical Nature of the Process

In light of the present findings, it is useful to consider why the mechanical aspect of the SCC mechanism has previously been rejected. Probably the most formidable argument is that there has been little evidence on the fracture surfaces to suggest a mechanical fracture process. Jacobs⁽⁷⁾ did report having evidence of mechanical rupture, but the corrosive nature of the "dimples" seemed to several others⁽²²⁾ to make this evidence inconclusive. In a similar set of experiments on a Al-Zn-Mg alloy, Sedriks, et al.⁽¹⁰⁾ reported no evidence of microvoid

coalescence in the stress-corrosion areas. However, they did find dimpled rupture on the part of the specimen that failed by the rapid mechanical fracture that terminated the test. Even though this rapid fracture part of the surface was exposed to the environment for some time, the dimples observed in that area were not attacked by corrosion. They then argued that if dimples existed in the SCC part of the fracture surface, these also should not have been corroded and hence should have been detected by either scanning electron microscopy or fractography. They therefore concluded that since no microvoids were in evidence, then the process must be purely anodic dissolution. The salient point of their argument is that the dimples forming under rapid crack growth would be as likely to corrode as dimples forming under SCC conditions, given equal time of exposure to the environment. However, there is no evidence to this effect and in fact, it is more likely that the conditions just behind a slowly growing crack would be more conducive to corrosion attack. Both the potential and the pH conditions would be considerably different from an unstressed, completely exposed fracture surface. Moreover, the present study has definitely established the fact that microvoid coalescence may be an integral part of the SCC mechanism in 7075-T6 aluminum. Thus, it is probable that Jacobs⁽⁷⁾ did observe microvoid coalescence associated with SCC. The fact that the microvoids were heavily corroded suggests that in many previous cases, obliteration of the true fracture surface details may have led some investigators to conclude, erroneously, that the mechanism was entirely void of any mechanical process.

Of course, it might be argued that the present data represent a relatively unique case and that this situation is not characteristic of other aluminum alloys. However, it is significant that the crack growth rate dependence on stress intensity is nearly identical to the K^2 dependence observed by Tetelman and McEvily⁽²³⁾ for Al-5.5Zn-2.5Mg in a neutral NaCl solution. The only difference was that the present growth rates were faster by a factor of four. Nevertheless, this is consistent with the fact that McHardy et al.⁽²⁴⁾ reports a factor of four decrease in time to failure for 7057-T6 stressed in an NaCl + AlCl₃ solution where the pH is less than two as compared to a neutral NaCl solution.

One final comment about the mechanical contribution concerns the absolute magnitude of the mechanical rupture process. Consider the size of the area swept out in a single jump, as indicated by the SWE amplitude. This 0.09×10^6 in² area would only be about 3% of the total cross-sectional area of a single grain. Thus, it would appear that the mechanical nature of the process, even at relatively high stress intensity levels, is a relatively localized process. This may not be so for finer grained materials or more susceptible higher strength alloys.

CONCLUSIONS

(1) The crack growth rate for the SCC process was strongly dependent on the temperature with an apparent activation energy of 11.2 kcal/mol. The crack growth rate was proportional to K^2 .

(2) Stress wave emission results showed that cracking was discontinuous and that the frequency of stress wave emissions increased with increasing stress intensity.

(3) Both mechanical and electrochemical fracture in the SCC region was intergranular, and the amount of dimpled rupture was proportional to K^2 .

(4) Crack growth during SCC is concluded to be a two-step process combining an electrochemical and mechanical process.

ACKNOWLEDGMENTS

The authors wish to thank Professor E. R. Parker for his continued encouragement and advice throughout this work.

This work was done under the auspices of the United States Atomic Energy Commission.

REFERENCES

1. G. Thomas and J. Nutting: J. Inst. of Metals, 88 (1959-60) pp. 81.
2. D. O. Sprowls and R. H. Brown: Proc. Conf. Fundamental Aspects of Stress Corrosion Cracking, National Assn. of Corrosion Eng., Houston (1969), p. 446.
3. A. J. Sedriks, P. W. Slattery and E. N. Pugh: Trans. Amer. Soc. for Metals, 62 (1969), pp. 815-818.
4. F. H. Haynie and W. K. Boyd: Proc. Conf. Fundamental Aspects of Stress Corrosion Cracking, National Assn. of Corrosion Eng., Houston (1969), p. 580.
5. A. J. Sedriks, J. A. S. Green, and D. L. Novak, Met. Trans.: 1, July 1970, p. 1815.
6. E. H. Dix, Jr.: Trans. AIME, 137 (1940), p. 11
7. A. J. Jacobs, Proc. Conf. Fundamental Aspects of Stress Corrosion Cracking, National Assn. of Corrosion Eng., Houston (1969), p. 530.
8. J. M. Krafft and J. H. Mulherin: Trans. Quart., ASM, 62 No. 1 (1969) p. 64.
9. A. F. Beck and P. R. Sperry: Proc. Conf. Fundamental Aspects of Stress Corrosion Cracking, National Assn. of Corrosion Eng., Houston (1969), p. 513.
10. A. J. Sedricks, P. W. Slattery, and E. N. Pugh: Trans. Quart. ASM 62, No. 1, (1969) p. 238.
11. M. O. Speidel: Proc. Conf. Fundamental Aspects of Stress Corrosion Cracking, National Assn. of Corrosion Eng., Houston (1969), p. 561.
12. P. N. T. Unwin and G. C. Smith: J. Inst. Metals, 97 (1969), p. 299.

13. Aluminum: Amer. Soc. for Metals, 1 (1967) p. 13.
14. W. Gruhl and H. Cordier: Z. Metallkunde, 55, 10 (1964) p. 577.
15. W. F. Brown and J. E. Srawley: Plane Strain Crack Toughness of High Strength Materials, ASTM, (Spec. Tech. Publ.) 410, Philadelphia, (1966).
16. W. W. Gerberich and C. E. Hartbower: Int. J. Fracture Mec. 3 (3) (1967).
17. C. E. Hartbower, W. W. Gerberich and P. P. Crimmins: Welding J. Res. Supp., 47, (10) (1968), p. 433.
18. C. E. Hartbower, W. W. Gerberich, H. Liebowitz: Eng. Frac. Mec. 1 (1968), p. 291.
19. W. W. Gerberich and J. D. Desai: Annual Technical Progress Report I, A.E.C. Contract AT-11-1-2212, to be submitted for publication.
20. E. N. Pugh and W. P. D. Jones: Metallurgia, 63, (1961), p. 3.
21. W. Gruhl and H. Cordier: Trans. Amer. Soc. for Metals, 56 (1963), p. 951.
22. A. J. Jacobs: Proc. Conf. Fundamental Aspects of Stress Corrosion Cracking, National Assn. of Corrosion Eng., Houston (1969), p. 559.
23. A. S. Tetelman and A. J. McEvily: Fracture of Structural Materials, J. Wiley and Sons, New York, (1967) p. 441.
24. J. M. McHardy and E. H. Hollingsworth: U. S. Navy Bureau of Naval Weapons Cont. NOW 65-0327f, final Report (1966).

FIGURE CAPTIONS

- Fig. 1. Schematic illustration of the experimental setup used to perform SCC tests and monitor stress wave emissions.
- Fig. 2. Typical microstructures of 7075 aluminum sheet. (A) and (B) as received material, (C) and (D) after cold rolling from .080" to .060" thickness, solution heat treating and quenching. A, B viewed from the top; B, D edge view perpendicular to the rolling direction.
- Fig. 3. Stress corrosion crack growth rate vs applied stress intensity for room temperature tests of 7075-T6 aluminum.
- Fig. 4. Stress corrosion crack growth rates vs temperature for three levels of applied stress intensity for 7075-T6 aluminum.
- Fig. 5. Oscillogram recordings of stress waves during room temperature SCC tests of 7075-T6 aluminum. (A) Background noise due to the testing machine and environment, no load applied; (B) SCC test with $K = 25,400 \text{ psi-in.}^{1/2}$; (C) SCC test with $K = 36,200 \text{ psi-in.}^{1/2}$; (D) SCC test with $K = 48,300 \text{ psi-in.}^{1/2}$.
- Fig. 6. Macroscopic fracture features of SCC test specimen. (A-B) pre-fatigued region, (B-C) slow crack growth region, (C-D) unstable crack growth.
- Fig. 7. Scanning electron micrographs illustrating the two different types of fracture surfaces observed in the slow crack growth regions of a SCC specimen tested at $K = 37,000 \text{ psi-in.}^{1/2}$. (A) relatively flat fracture surface indicative of anodic dissolution, and (B) dimpled rupture fracture surface indicative of discontinuous jumping, or tearing.

Fig. 8. Scanning electron micrographs of a SCC specimen tested at an applied stress intensity of $26,740 \text{ psi-in.}^{1/2}$.

Fig. 9. Scanning electron micrographs of a SCC specimen tested at an applied stress intensity of $49,600 \text{ psi-in.}^{1/2}$.

Fig. 10. Scanning electron micrograph showing a residual deposit of the test solution. (A) and (B) deposits on the actual fracture surface, and (C) and (D) deposits evaporated on a nickel plate for comparison.

Table 1. Mechanical properties of 7075-T6 aluminum

	Yield Strength (0.2% offset) (psi)	Ultimate Strength (psi)	% Elong. (1.0 in. gage)	% Reduction of area
As received material	71,500 ± 1100	80,700 ± 400	11.6 ± 1.6	28 ± 8
Rolled, solution H.T., and aged	56,800 ± 1200	79,000 ± 1200	15.2 ± 1.8	26 ± 3

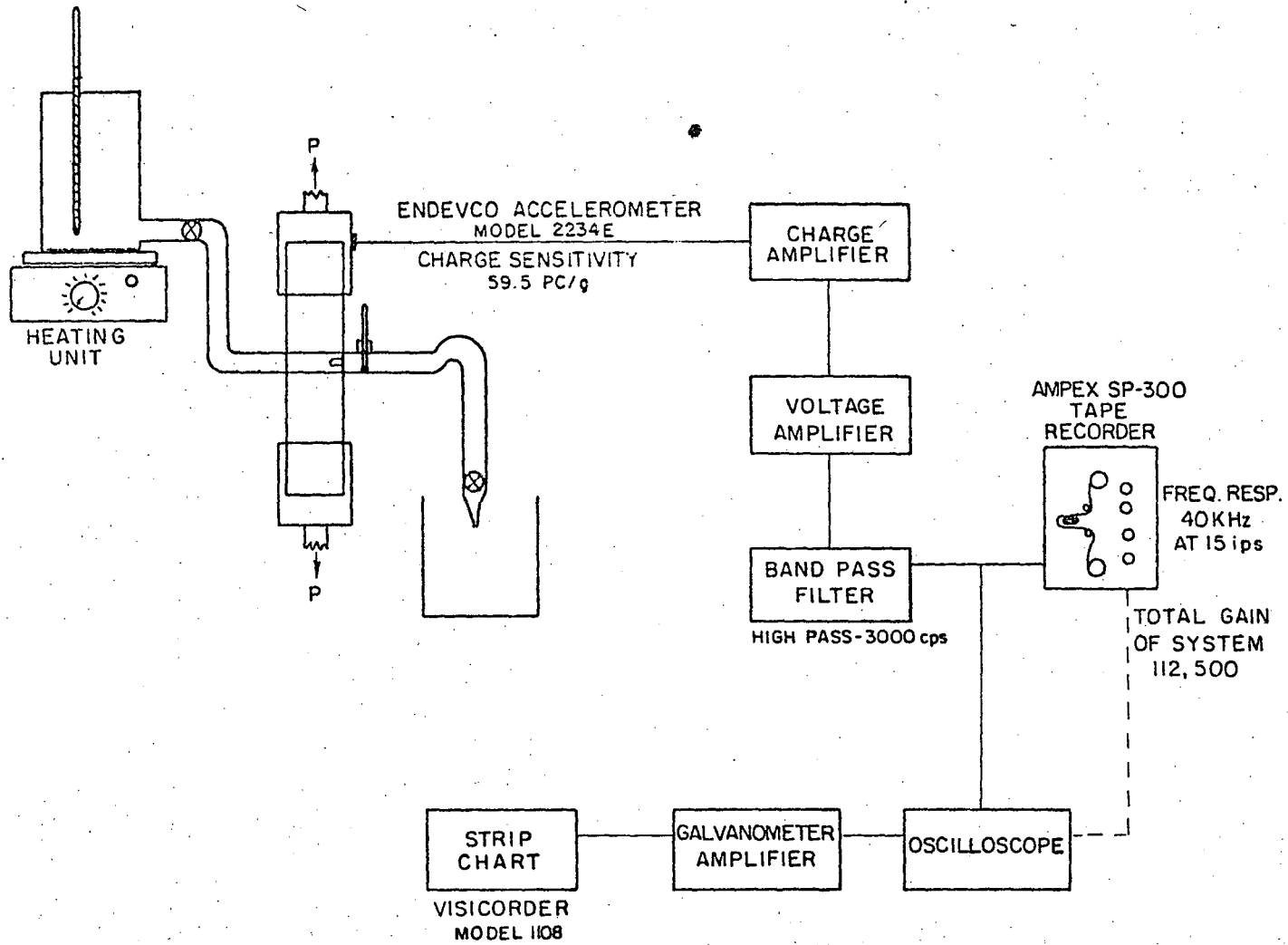
Table 2. SCC data from crack propagation tests

Test Temp. T (°C)	Stress Intensities			Time Increment Δt (min)	Crack Increment Δa (in.)	Crack Growth Rate da/dt (in./min)
	K_o (psi-in. ^{1/2})	K_f (psi-in. ^{1/2})	K_{AVE} (psi-in. ^{1/2})			
10	36,100	39,500	37,800	47.0	.048	.0010
23	45,400	50,700	48,050	14.8	.070	.0047
23	44,700	50,000	47,400	5.2	.070	.0135
23	34,700	38,500	36,600	19.3	.070	.0036
23	36,500	38,500	37,500	21.4	.043	.0020
23	32,200	36,800	35,500	14.7	.055	.0037
23	27,600	40,000	33,800	73.0	.270	.0037
23	31,700	34,700	33,200	25.5	.065	.0026
23	24,000	27,500	25,800	26.0	.090	.0035
23	23,800	26,300	25,000	47.0	.077	.0016
23	21,800	25,700	23,800	60.0	.110	.0018
23	30,600	52,800	41,700	67.8	.405	.0060
22	29,000	32,400	30,700	26.7	.080	.0030
23	14,900	20,500	17,700	230.0	.195	.00085
23	9,250	9,250	9,250	328.0	.000	.0000
23	38,900	39,900	39,400	13.0	.065	.0050
23	15,600	18,800	17,200	204.0	.070	.00034
32	46,900	49,900	48,400	5.2	.045	.0086
33	35,100	35,500	35,300	6.7	.025	.0037
33	23,800	25,000	24,400	7.6	.040	.0052
43	34,400	37,600	36,000	4.2	.063	.0150
43	25,600	27,500	26,500	9.4	.050	.0053
43	25,300	26,500	25,900	5.3	.045	.0085
48	47,700	51,500	49,600	1.4	.055	.0402
53	34,800	38,800	36,800	2.8	.070	.0250
53	24,900	28,500	26,700	7.5	.090	.0120
53	24,600	27,400	26,000	11.4	.080	.0070
62	26,200	25,200	25,700	0.8	.010	.0122
62	25,300	25,300	25,300	1.2	.025	.0220
68	47,300	48,700	48,000	1.1	.076	.0724
73	36,100	37,300	36,700	0.9	.045	.0500
73	25,500	25,600	25,550	1.0	.020	.0200
73	24,600	24,400	24,500	0.75	.020	.0267

Table 3. Stress-wave and fractographic observations

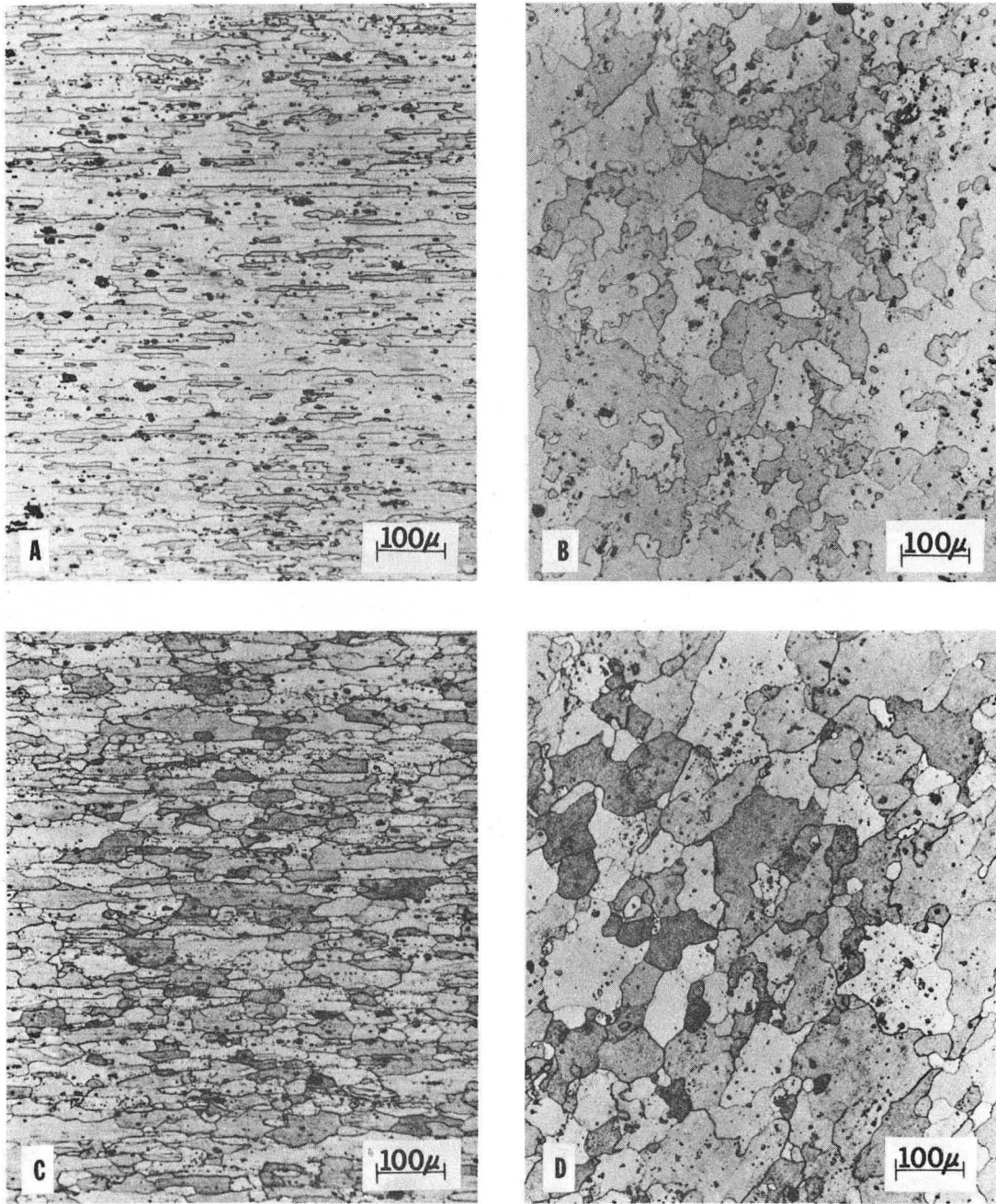
K_{AVE} , psi-in. ^{1/2}	T, °C	SWE/sec	Δt_s , sec	Dimple Rupture, %
25,400	23	2.0	0.5	20
36,200	33	6.6	0.151	33
48,300	23	11.0	0.091	80

K_{AVE} , psi-in. ^{1/2}	da/dt, in./sec x 10 ⁵	SWE Amplitude, g, ft/sec ² x 10 ⁴ , ΔA , in. ² x 10 ⁶
25,400	2.7	2.3 0.078
36,200	10	3.6 0.085
48,300	12	5.7 0.113



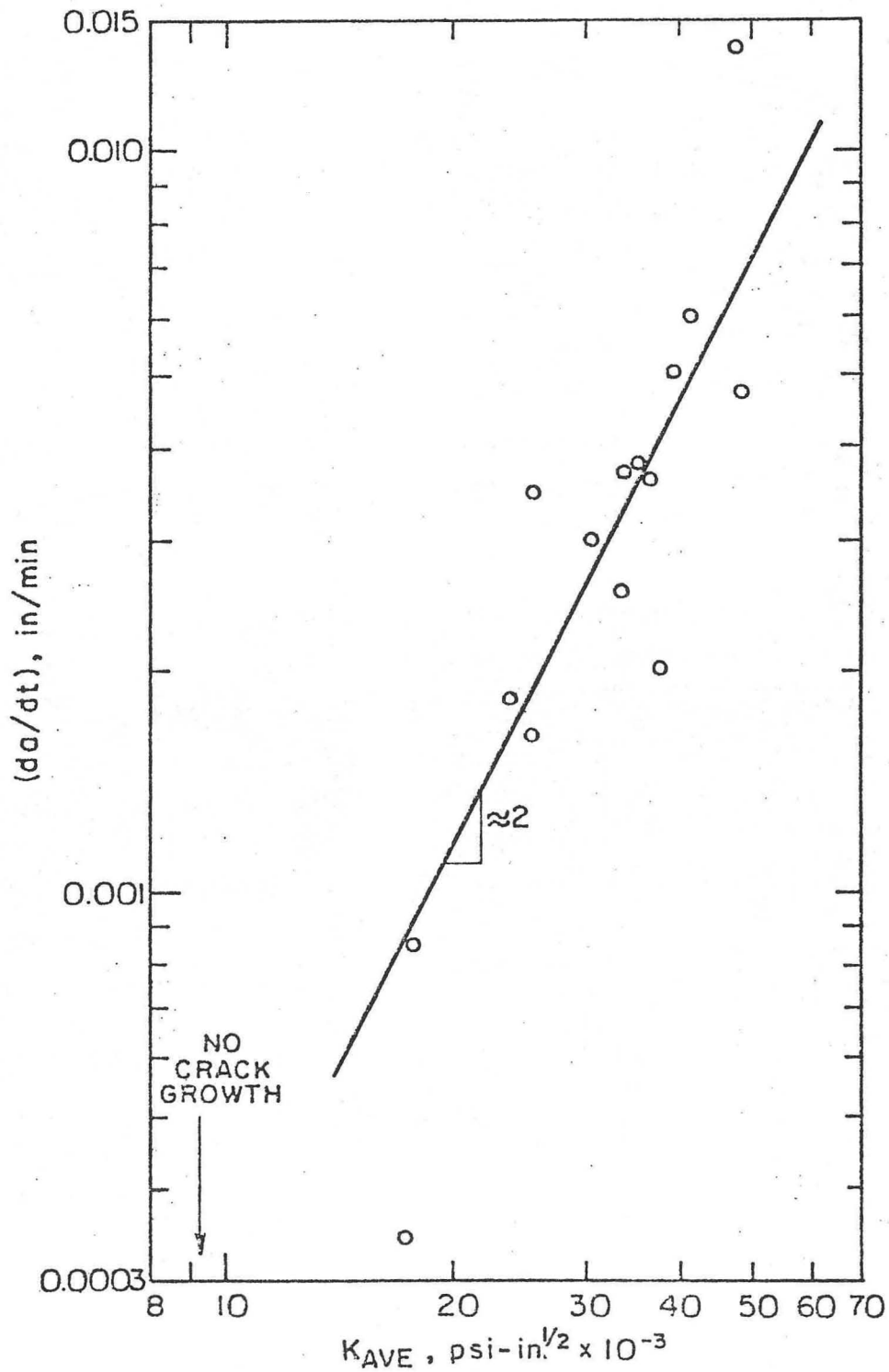
XBL 708-6421

Fig. 1.



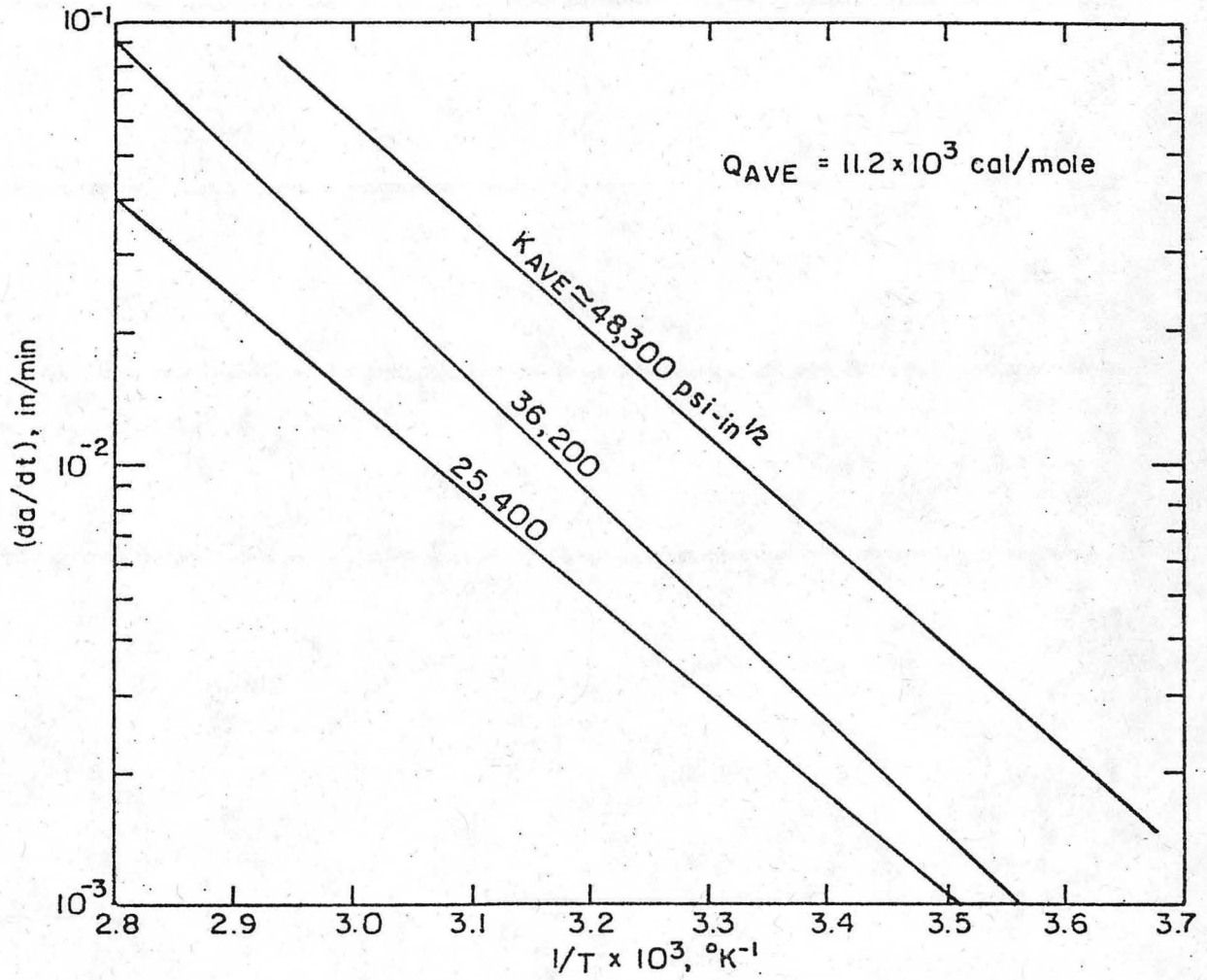
XBB 708-3810

Fig. 2



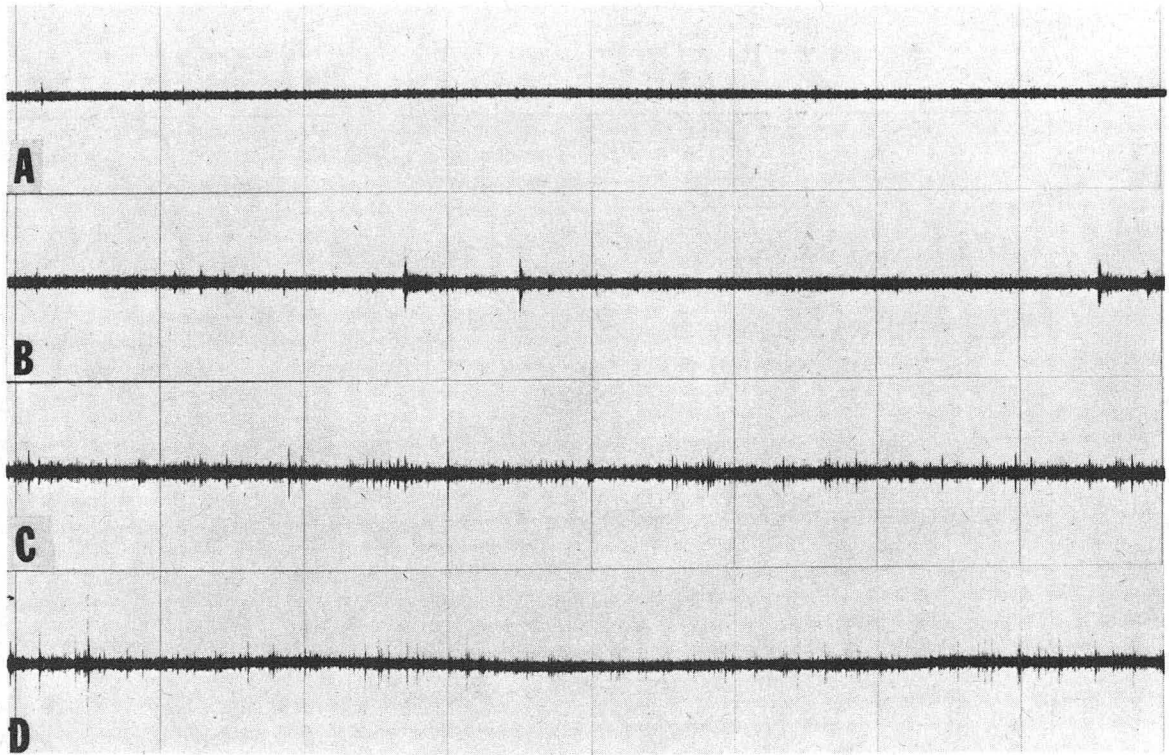
XBL708-6422

Fig. 3



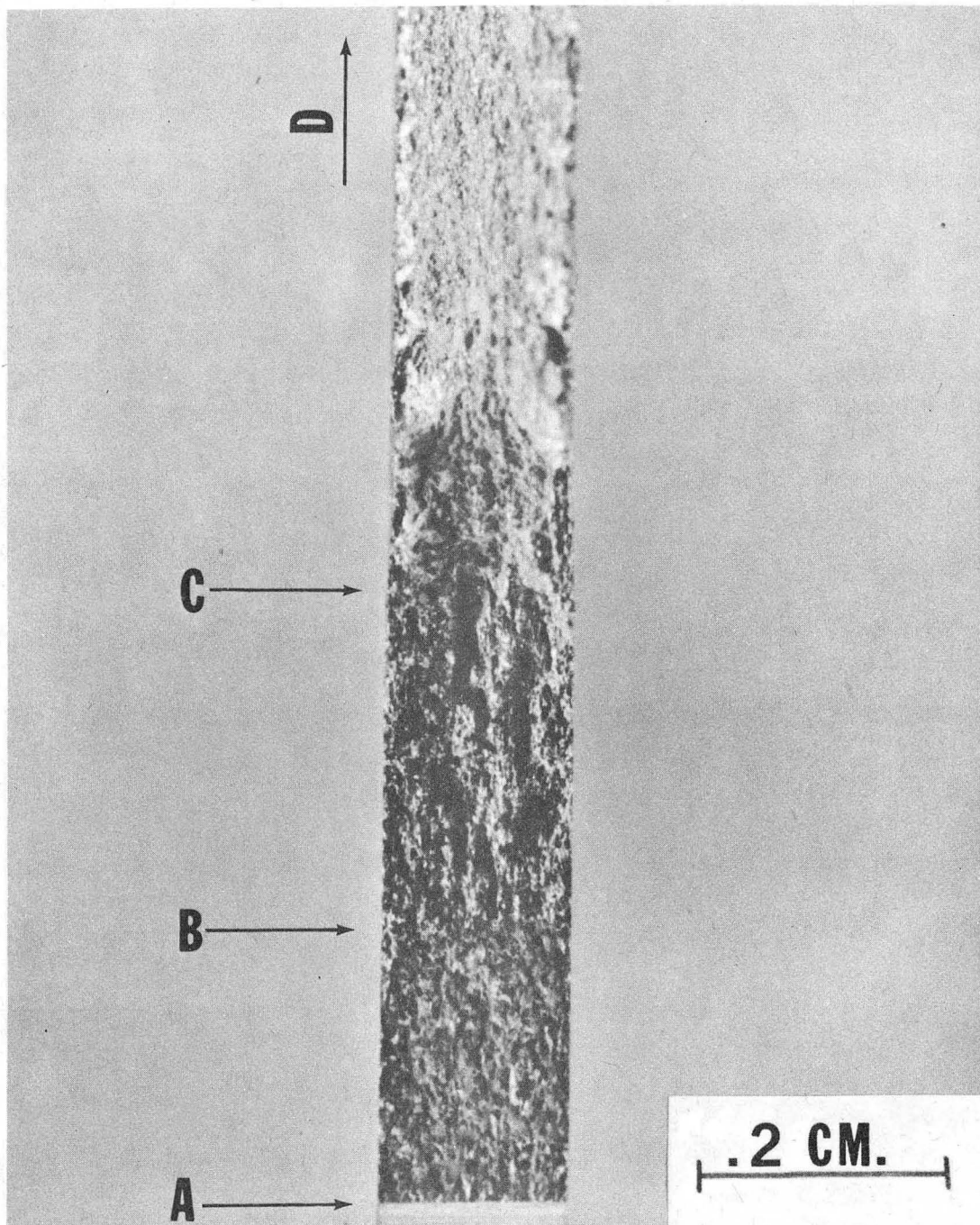
XBL708-6417

Fig. 4



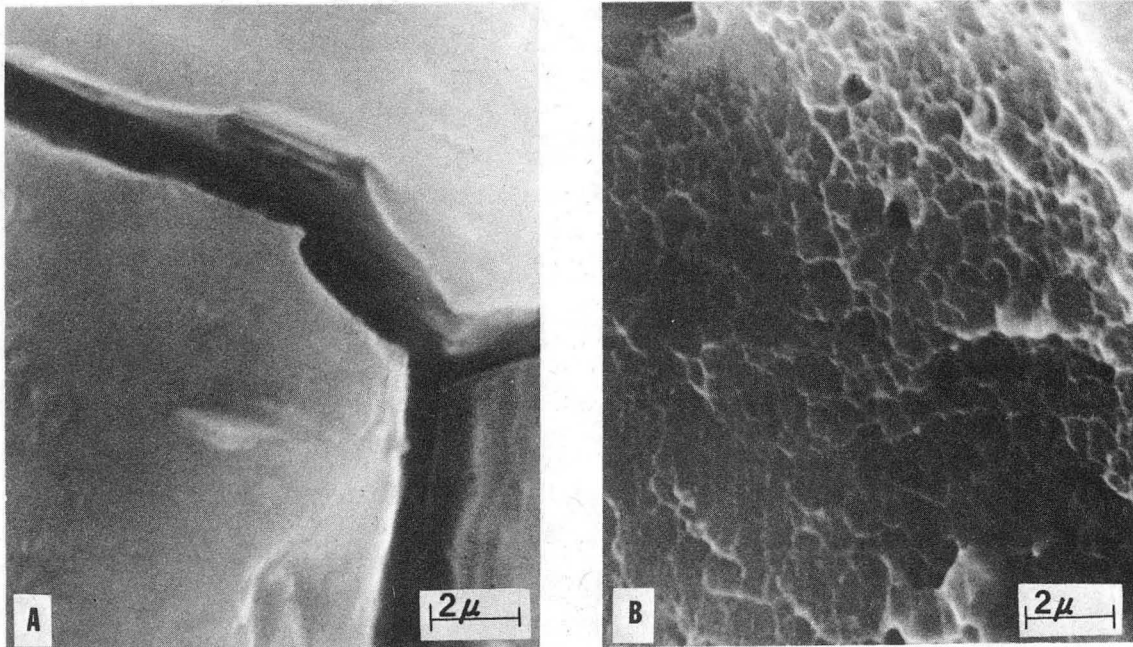
XBB 709-4177

Fig. 5



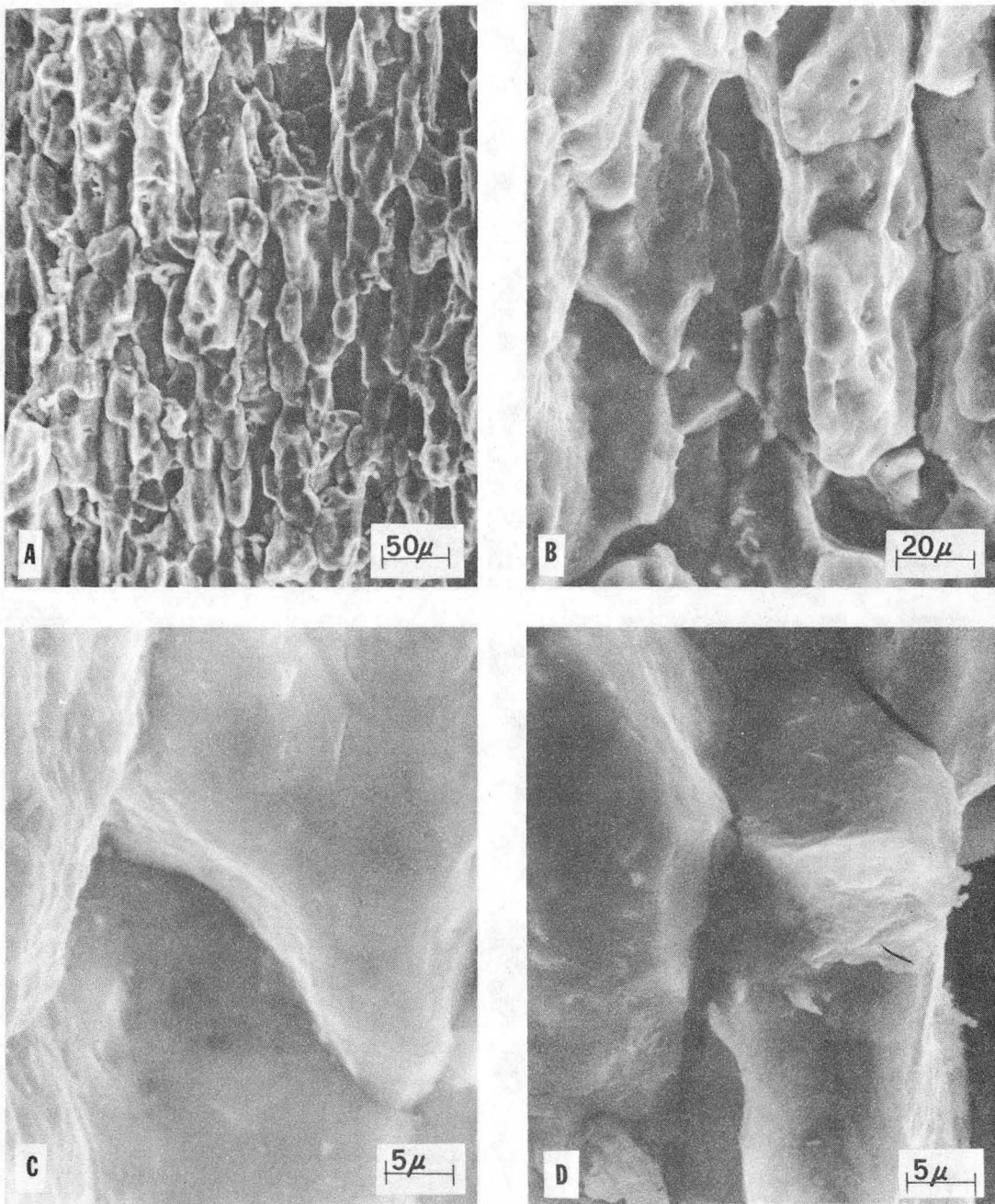
XBB 709-4179

Fig. 6



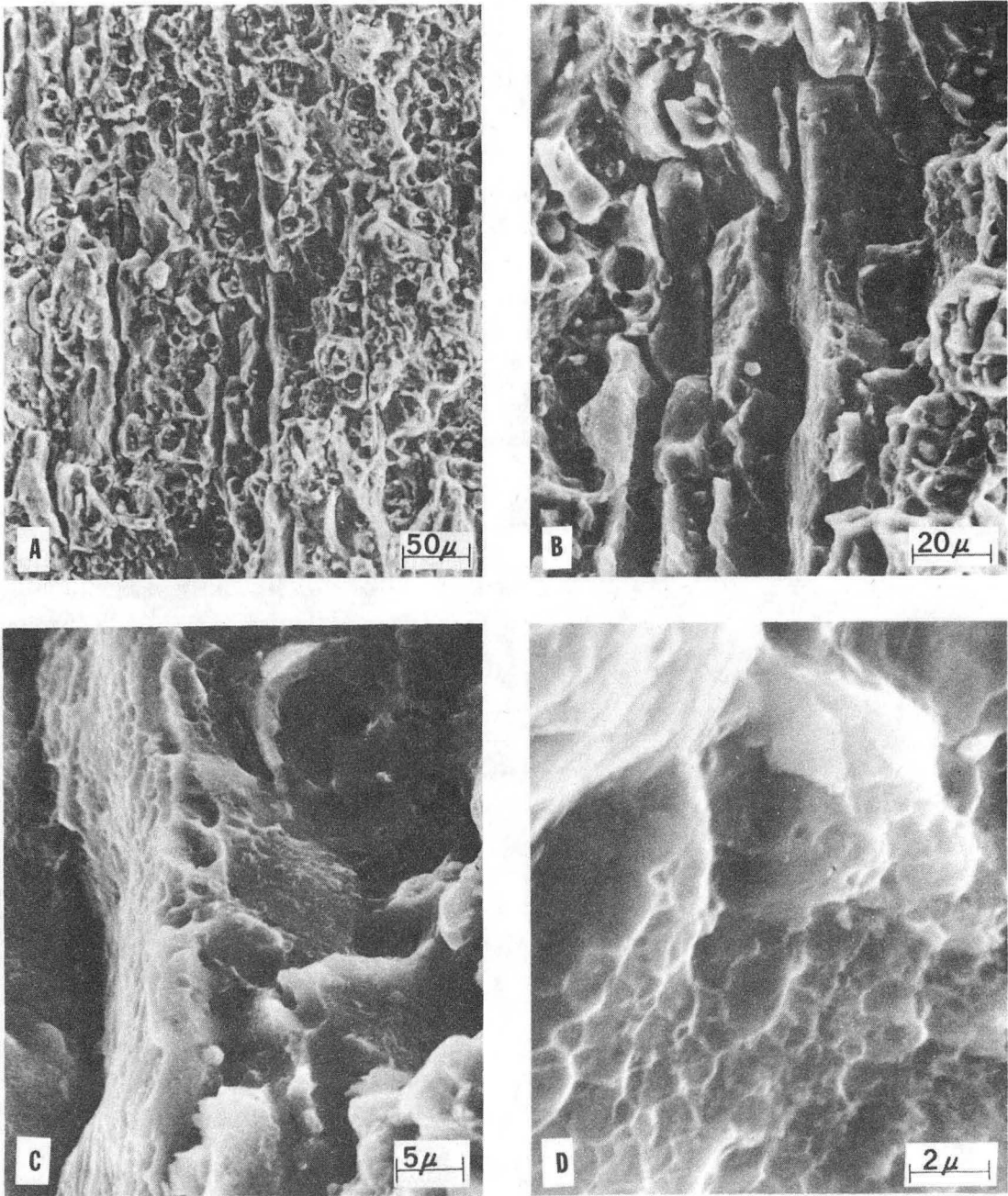
XBB 709-4176

Fig. 7



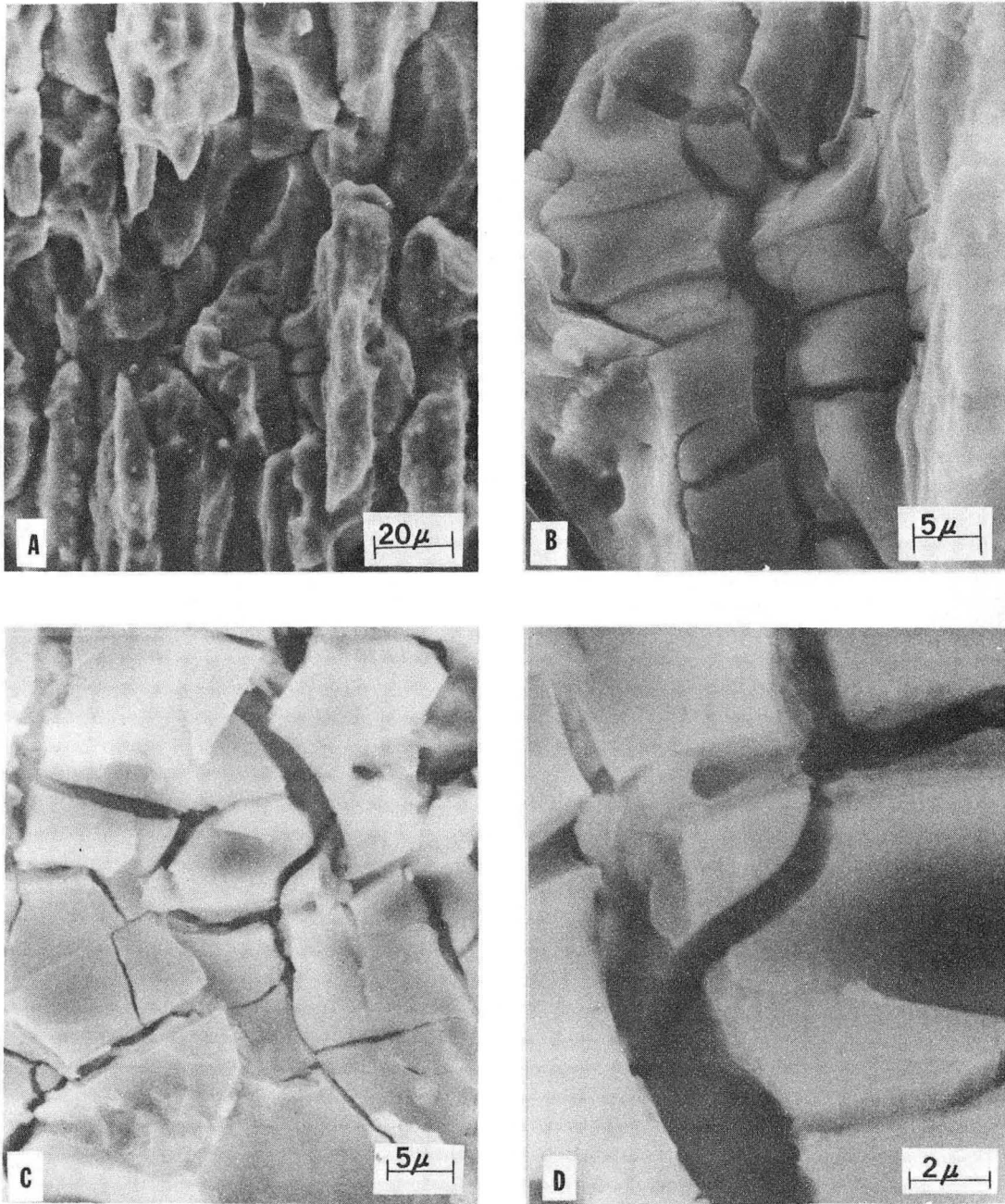
XBB 708-3813

Fig. 8



XBB 708-3814

Fig. 9



XBB 709-4178

Fig.10

LEGAL NOTICE

This report was prepared as an account of work sponsored by the United States Government. Neither the United States nor the United States Atomic Energy Commission, nor any of their employees, nor any of their contractors, subcontractors, or their employees, makes any warranty, express or implied, or assumes any legal liability or responsibility for the accuracy, completeness or usefulness of any information, apparatus, product or process disclosed, or represents that its use would not infringe privately owned rights.

TECHNICAL INFORMATION DIVISION
LAWRENCE BERKELEY LABORATORY
UNIVERSITY OF CALIFORNIA
BERKELEY, CALIFORNIA 94720